Supporting information

Tunable Synthesis of Ag Films at Ionic Liquids/Aqueous Interface

Kaisheng Yao,[a,b] Weiwei Lu,[a] Xinying Li[a] and Jianji Wang*[a] Jiongliang Yuan[c]

[a] School of Chemistry and Environmental Science, Key Laboratory of Green Chemical Media and Reactions, Ministry of Education, Henan Normal University, Xinxiang, Henan 453007, P. R. China. E-mail: jwang@henannu.edu.cn

[b] College of Chemistry and Chemical Engineering, Lanzhou University, Lanzhou, Gansu 730000, P. R. China

[c] Department of Environmental Science and Engineering, Beijing University of Chemical Technology, Beijing 100029, P. R. China.

* Corresponding author
E-mail: jwang@henannu.edu.cn (Prof J. Wang)
Tel: +86-373-3325805
Fax: +86-373-3326445

Experimental Section

Materials: 1-Methylimidazole (C.P.) and a series of alkyl bromides were purchased from Linhai Kaile Chem. Co. and Alfa Aesar, respectively. These chemicals were distilled before use. KPF_6 (99%), tetrafluoroboric acid (48% solution in water) and *o*-ethoxyaniline (98%) were purchased from Aladdin Chem. Co.; $LiTf_2N$ (≥99%) was purchased from Zhejiang Jiuzhou Pharmaceutical Co.; Silver nitrate（≥99.9%), trichloromethane（≥99%) and ethanol were from Sinopharm Chem. Reagent Co. These Chemicals were used without further purification. Double distilled water was used throughout the experiments.

Synthesis of the ILs: The used ILs $[C_4mim][PF_6]$, $[C_6mim][PF_6]$, $[C_8mim][PF_6]$, $[C_{10}mim][PF_6]$, $[C_{10}mim][Tf_2N]$, and $[C_{10}mim][BF_4]$ were prepared and purified by using the procedure described in the literature.[1]

Synthesis of the Ag films: Ag films were deposited at the interface of immiscible ILs and H_2O, and their synthetic reactions were illustrated in Scheme 1. In a typical synthesis, 4 ml of 10 mM aqueous $AgNO_3$ solution was slowly added onto 2 ml of 100 mM *o*-ethoxyaniline in ILs along the glass wall of vial (2.2 cm diameter). The system was kept in a reactor with a circulating water jacket at 40 ℃ for 5 h without disturbance. The Ag films were gradually formed at the ILs-H_2O interface. They were transferred to various substrates previously placed on the bottom of the reactor by removing the IL phase with a syringe, and then were immersed in an aqueous solution containing 50-90 wt% ethanol for 24 h to extract the residual ILs before characterization. Changed morphologies can be obtained by employing different ILs-H_2O reaction systems.

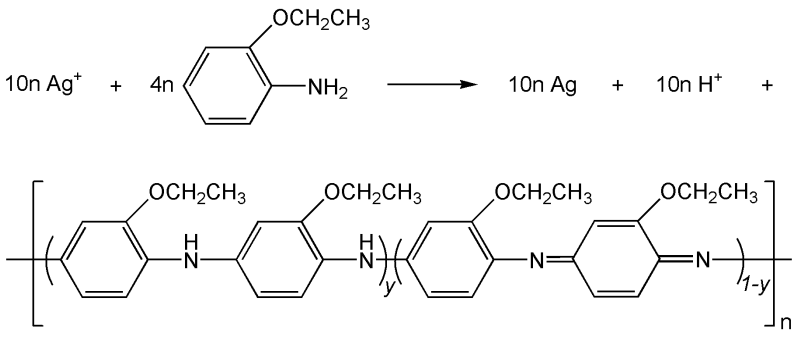

Scheme 1 Reaction conversion of the preparation of Ag films at the ILs-H_2O interface.

Characterizations: Morphologies and elemental composition of the films, deposited on silicon wafer or glass slide, were observed and analyzed on a JEOL JSM-6390LV scanning electron microscope (SEM) and on a Genesis XM2 energy-dispersive X-ray spectroscopy (EDX) equipped on the SEM, respectively. Transmission electron microscopy (TEM) and high resolution transmission electron microscopy (HRTEM) were taken on a JEOL 2100 transmission electron microscope at an acceleration voltage of 200 kV. The specimens for the HRTEM measurements were prepared by ultrasonic dispersion of the as-prepared films with ethanol. Then, a drop of the solution was deposited onto a carbon-coated copper grid and dried at room temperature before the analysis. Fourier transform infrared (FTIR) spectra were recorded on a Necolet Nexus spectrometer with KBr pellets. X-ray diffraction (XRD) patterns of the samples were recorded on a Bruker D8 Advance X-ray diffractometer (Cu irradiation, λ = 0.154056 nm) in 2θ ranging from 30° to 70°.

SEM image and FT-IR spectrum of the POEA belts:

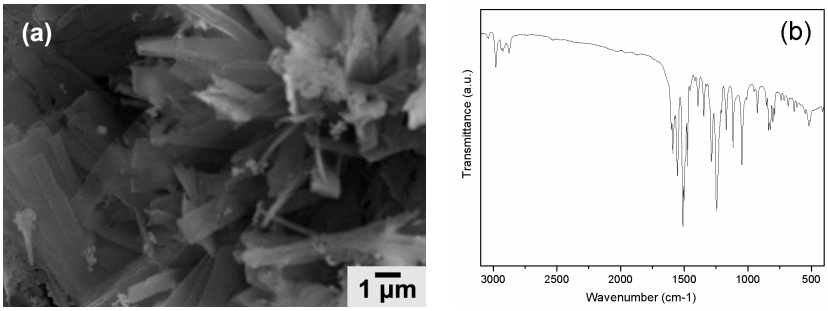

Fig. S1 (a) SEM image and (b) FT-IR spectra of POEA belts.

Fig. S1(a) presents SEM image of the belt-like structures of POEA generated at the studied ILs-H_2O interfaces in the course of reducing Ag^+. Fig. S1(b) shows the FTIR spectrum of POEA belts polymerized during the formation of Ag films. The absorption related to the C=N on the quinoid ring and the C=C stretching on the benzenoid ring appear at 1552 cm^{-1} and 1510 cm^{-1}, respectively. The bands at 1286 cm^{-1} and 1247 cm^{-1} are attributed to C-N and C-O stretching absorption, respectively. The band at 1169 cm^{-1} is assigned to the N=Q=N vibration (Q = quinoniod), and the band at 1117 cm^{-1} attributes to C-H in-plane bending vibrations. In addition, the bands at 1392 cm^{-1}, 2873 cm^{-1} and 2935 cm^{-1} are due to $-CH_3$-substituted group, while the bands at 2981 cm^{-1} and 3045 cm^{-1} originate from the C-H

stretch on the benzenoid ring. The bands from 1000 to 400 cm^{-1} belong to the *o*-substituted aromatic ring.[2]

SAED patterns of the nanoplates:

The typical SAED patterns were obtained by aligning the beam perpendicular to the flat facets of nanoplates. It can be seen that the nanoplate is a single crystal. The hexagonal symmetry diffraction spot pattern implies that the nanoplates are bounded mainly by (111) planes.[3] Three sets of spots could be identified based on the *d*-spacing: the strongest intensity spot with a spacing of 1.44 Å (marked by a square) corresponds to the {220} reflection of fcc Ag. The outer set with a lattice spacing of 0.83 Å (marked by a triangle) can be indexed to the {422} Bragg reflection. The inner set (marked by a circle) with a spacing of 2.5 Å can be ascribed to the forbidden 1/3{422} reflection.[3] According to the zone law:

$$u:v:w=\begin{vmatrix}k_1 & l_1\\ k_2 & l_2\end{vmatrix}:\begin{vmatrix}l_1 & h_1\\ l_2 & h_2\end{vmatrix}:\begin{vmatrix}h_1 & k_1\\ h_2 & k_2\end{vmatrix}=\begin{vmatrix}2 & 0\\ 2 & 2\end{vmatrix}:\begin{vmatrix}0 & -2\\ 2 & -4\end{vmatrix}:\begin{vmatrix}-2 & 2\\ -4 & 2\end{vmatrix}=1:1:1$$

it can be concluded that the top and bottom of the nanoplate are bounded by (111) planes. The crystal axis of the nanoplate is the [111] zone axis and the nanoplate is grown along the [110] and/or [100] direction.[3,4]

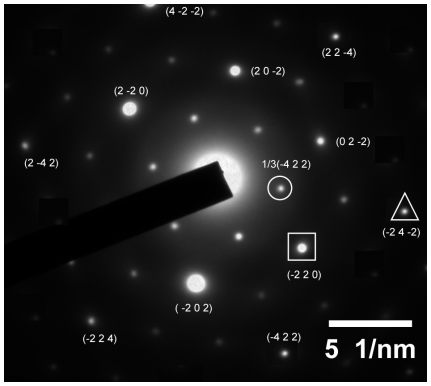

Fig. S2 The SAED patterns of nanoplates by aligning the beam perpendicular to its flat facets, the spots circumscribed by square, triangle, and circle correspond to the {220}, {422} and forbidden (1/3){422} reflections, respectively.

XRD patterns for the different Ag products:

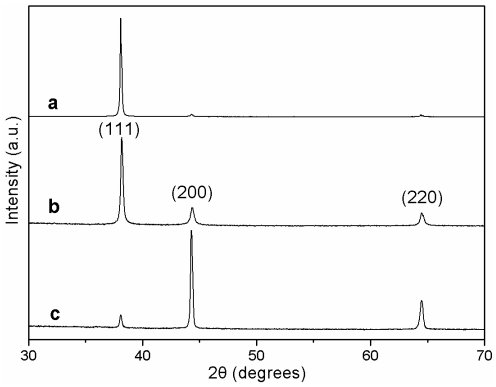

Fig. S3 XRD patterns of the Ag films prepared at different ILs-H_2O interface: (a) [C_{10}mim][PF_6]-H_2O, (b) [C_{10}mim][Tf_2N]-H_2O, and (c) [C_{10}mim][BF_4]-H_2O.

Fig. S2 displays the X-ray diffraction (XRD) patterns of Ag films prepared at the interface of [C_{10}mim][PF_6]-H_2O, [C_{10}mim][Tf_2N]-H_2O and [C_{10}mim][BF_4]-H_2O, respectively. The peaks for all the samples can be indexed to diffraction from the (111), (200) and (220) planes of the face-centered cubic (fcc) Ag (JCPDS card no. 04-0783). Notably, the ratio (0.024) between intensity of the (200) and (111) diffraction peaks in Fig. S2a is unusually lower than the corresponding conventional value (0.4). This demonstrates that the Ag nanoplates are mainly dominated by (111) facets, and thus their (111) planes tend to be preferentially oriented parallel to the surface of the supporting substrate.[5] The ratio (0.180) between intensity of the (200) and (111) diffraction peaks in Fig. S2b is also lower than conventional value (0.4)**.** However, that in Fig.S2c is much higher than the conventional value (7.35 versus 0.4), indicating that the products are abundant in (100) facets.[6] These results are in good agreement with the electron microscope analysis of the corresponding samples.

EDX spectra for different Ag products:

Fig. S3 shows EDX spectra of the as-prepared products at different ILs-H_2O interfaces. It is indicated that all the products consist exclusively of Au, and the additional signals of Si arise from the substrate of silicon wafer.

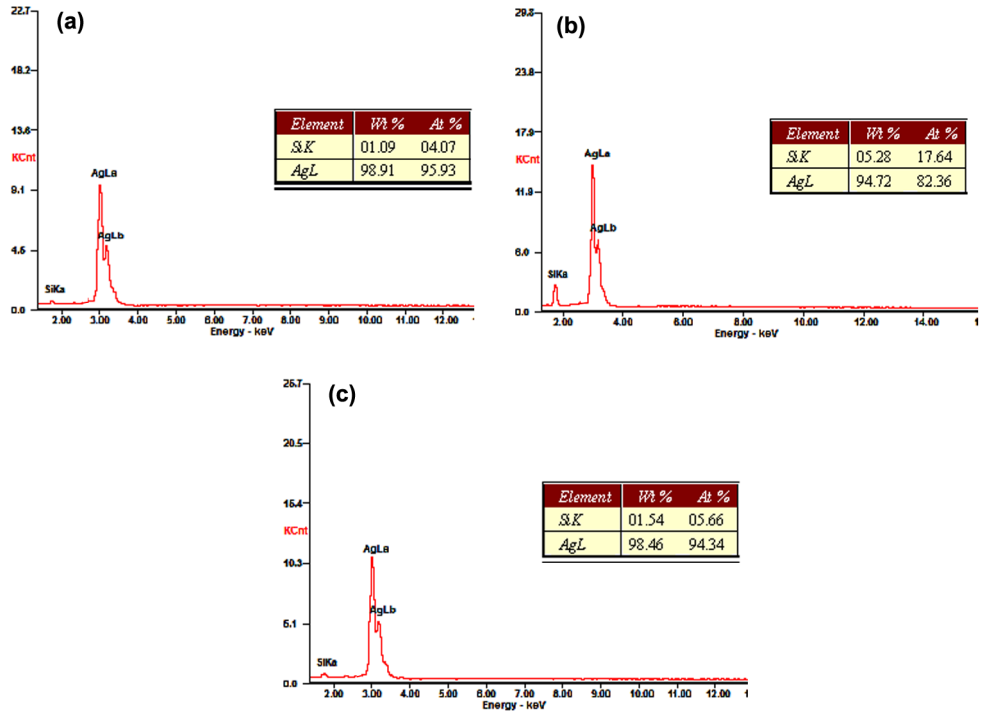

Fig. S4 EDX spectra of the Ag films prepared at different ILs-H_2O interface: (a) $[C_{10}mim][PF_6]$-H_2O, (b) $[C_{10}mim][Tf_2N]$-H_2O and (c) $[C_{10}mim][BF_4]$-H_2O.

SEM image of the samples obtained at the $CHCl_3$-H_2O interface:

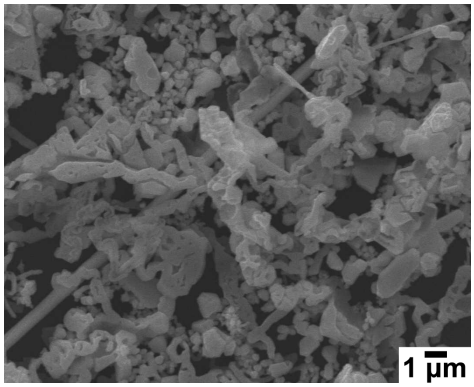

Fig. S5 SEM image of the sample prepared at the $CHCl_3$-H_2O interface.

SEM images of the samples prepared at ILs-H_2O interface with different alkyl chain lengths of cations of the ILs:

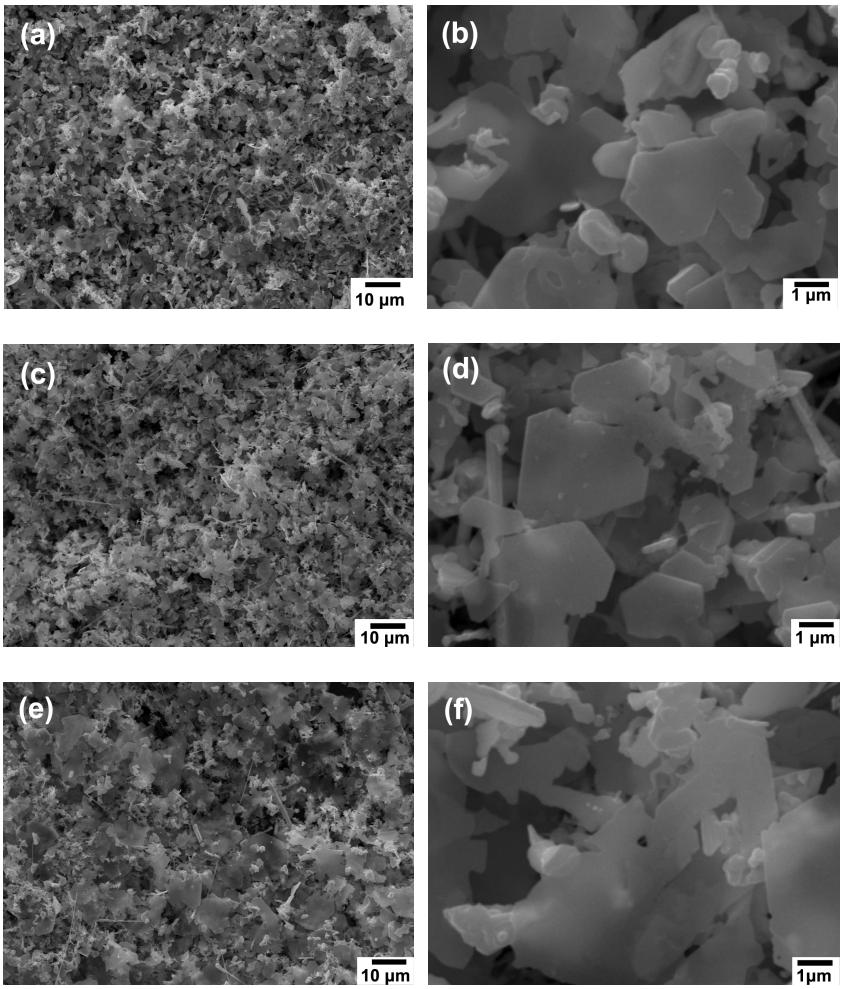

Fig. S6 SEM images of the Ag films synthesized at different ILs-H_2O interfaces: (a, c, e) and (b, d, f) correspond to low- and high-magnification images of the films prepared at $[C_4mim][PF_6]$-, $[C_6mim][PF_6]$-, and $[C_8mim][PF_6]$-H_2O interfaces, respectively.

Growth processes of the Ag nanobelts and quasi-cubes:

Fig. 4b shows TEM images of the Ag particles prepared at $[C_{10}mim][Tf_2N]$-H_2O interface and different reaction times. At the initial reaction time of 30 min, some irregular nanoparticles and small nanaoplates were observed (Fig. 4bi). As the reaction was prolonged to 1 h, some connected nanoparticles and short nanobelts appeared (Fig. 4bii), and they further grew into longer nanobelts with the increase of reaction time to 2 h (Fig. 4biii). When the reaction time was up to 3 h, the belt-like Ag structures with smooth edges were generated (Fig. 4biv). The growth process of quasi-cubes was shown in Fig. 4c. It can be seen that some

small and elongated Ag nanoparticles were formed at the initial reaction time of 30 min (Fig. 4ci). With the increase of reaction time, they gradually aggregated and grew into larger particles as shown in Fig. 4cii and iii. As the reaction time was prolonged to 3 h, large particles with smooth surfaces were formed (Fig. 4civ). Further growth led to the formation of quasi-cubes (Fig.3). During the formation of different morphologies of the Ag particles, the liquid-liquid interface, high viscosity and anionic nature of the ILs, and microstructures of the ILs-H_2O interfaces might play important roles.

Molecular dynamics simulation:

Molecular dynamics (MD) simulation in canonical ensemble (constant atom number, volume and temperature, NVT) was employed to calculate the interaction energies of OEA and [C_{10}mim][PF_6] with different Ag crystalline planes. The simulation method and structural analysis are similar to those reported in literature.[7] In the calculations of the interaction energies of OEA and [C_{10}mim][PF_6] with Ag crystalline planes of (100), (110) and (111), three models were established: (1) the three-dimensional model consisting of one Ag crystal plane and a certain amount of OEA molecules on the Ag surfaces; (2) Ag crystal plane only; and (3) OEA molecules only. All simulations were performed by the Discover Module of Materials Studio, and the COMPASS force field was used to calculate the interaction potential energy. All the systems were subjected to energy minimization for the structural optimization before MD simulation. The simulation data were collected in the last 100 ps for statistical and structural analysis.

The interaction energies (U) were calculated for different systems of molecule-Ag plane by using equation (1)

$$U = E_{\text{total}} - E_{\text{surface}} - E_{\text{OEA (or IL)}} \qquad (1)$$

where E_{total} is the total energy of the crystal surface and OEA or IL, E_{surface} is the surface energy after removal of OEA or IL, $E_{\text{OEA (or IL)}}$ is the energy after removal of the surface. A negative value means an attractive interaction while a positive value indicates a repulsive interaction. The calculated interaction energies of OEA and [C_{10}mim][PF_6] with different Ag crystal surfaces were summarized in Table S1. Unfortunately, it can be seen that the differences in the interaction energies of OEA and [C_{10}mim][PF_6] with (100) and (111) were

too small to reasonably explain the formation of plate-like nanostructures. This demonstrates that the mechanism of platelike structures was not controlled by thermodynamics.

In addition, we also tried to calculate the interaction energies of $[C_{10}mim][Tf_2N]$ and $[C_{10}mim][BF_4]$ with different Ag planes. Unfortunately, no force field parameters are available for $[C_{10}mim][Tf_2N]$ and $[C_{10}mim][BF_4]$ in the MD software, and these parameters are not allowed to be added in the COMPASS force fields of the software.

Table S1. The calculated interaction energies (kcal mol^{-1}) for OEA- and IL-Ag plane systems.

	$[C_{10}mim][PF_6]$	OEA
Ag(100)	-192.2	-109.4
Ag(110)	-122.2	-67.6
Ag(111)	-199.4	-124.8

FTIR spectra of the pure ILs and the Ag /ILs:

FTIR measurements of the pure ILs and their corresponding Ag/ILs were also performed to study growth mechanism of the Ag particles. Compared with the FTIR spectra of pure ILs of $[C_{10}mim][PF_6]$ and $[C_{10}mim][Tf_2N]$, little change was observed for the spectra of the Ag nanoplates/$[C_{10}mim][PF_6]$ and nanobelts/$[C_{10}mim][Tf_2N]$ (Fig. S6-7 and Tables S2-3). This indicates that the interactions of these two ILs with corresponding Ag products are rather weak. Fig. S8 and Table S4 show the FTIR spectra of pure $[C_{10}mim][BF_4]$ and Ag cubes/$[C_{10}mim][BF_4]$ as well as their main absorption bands. The absorption peak at 1059 cm^{-1}, ascribed to the $[BF_4]^-$ stretching vibration, was weakened and broadened after the quasi-cubes were formed at $[C_{10}mim][BF_4]$-H_2O interface, demonstrating the strong interactions between $[C_{10}mim][BF_4]$ and Ag quasi-cubes. In addition, the interaction of $[BF_4]^-$ with Ag cubes can also be corroborated by examining the change in the C-H stretching vibration ($\nu_{C\text{-}H}$) modes of the imidazolium ring at 3161 and 3122 cm^{-1}. It can be seen that $\nu_{C\text{-}H}$ peaks in Fig. S8a are considerably broadened and weakened in Fig. S8b and give rise to obvious shifts to lower wavenumber of 16 and 36 cm^{-1}, respectively. These changes probably originate from the π-π stack interaction of the positive-charged imidazolium rings which

decreases the electronic density of C-H bond on the ring.[8] Since the $\nu_{C\text{-}H}$ modes of the imidazolium ring barely change for the Ag nanoplates/$[C_{10}mim][PF_6]$ and nanobelts/$[C_{10}mim][Tf_2N]$ systems, it is reasonable to state that the changes in the $\nu_{C\text{-}H}$ modes of the imidazolium ring for Ag cubes/$[C_{10}mim][BF_4]$ was caused by the change in the interaction between $[BF_4]^-$ and Ag cubes. Thus, the changes in both $[BF_4]^-$ stretching vibration and the $\nu_{C\text{-}H}$ modes of the imidazolium ring for Ag cubes/$[C_{10}mim][BF_4]$ indicates that $[BF_4]^-$ anions have strong interactions with Ag and $[C_{10}mim][BF_4]$, just like an surfactant, plays a template role during the formation of Ag cubes.

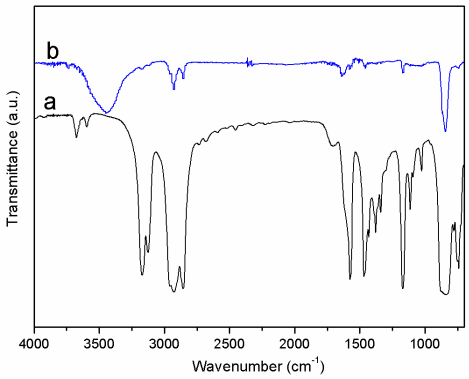

Fig. S7 FT-IR spectra of (a) the pure $[C_{10}mim][PF_6]$ and (b) the Ag nanoplate/$[C_{10}mim][PF_6]$.

Table S2. The main FTIR absorption bands of pure $[C_{10}mim][PF_6]$ and Ag nanoplates/$[C_{10}mim][PF_6]$[a]

Wavelength of the bands (cm^{-1})		Vibration
Pure $[C_{10}mim][PF_6]$	Ag nanoplates/$[C_{10}mim][PF_6]$	
3170, 3124	3170, 3126	ν (C-H) imidazole ring, str
2956, 2926, 2856	2954, 2926, 2854	ν (C-H) alkyl chains, str
1576, 1468	1576, 1471	Imidazole ring skeleton, str sym
839	843	ν(P-F), str

[a] Abbreviations: str, stretching; sym, symmetrical.

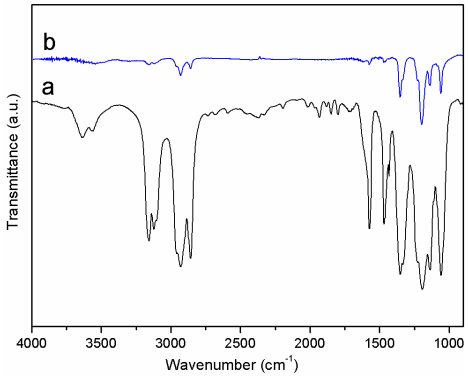

Fig. S8 FT-IR spectra of (a) the pure $[C_{10}mim][Tf_2N]$ and (b) the Ag nanobelts/$[C_{10}mim][Tf_2N]$.

Table S3. The main FTIR absorption bands of pure $[C_{10}mim][Tf_2N]$ and Ag nanobelts/$[C_{10}mim][Tf_2N]$[a]

Wavelength of the bands (cm^{-1})		Vibration
Pure $[C_{10}mim][Tf_2N]$	Ag nanobelts/$[C_{10}mim][Tf_2N]$	
3157, 3122	3155, 3118	*v* (C-H) imidazole ring, str
2953, 2927, 2856	2953, 2929, 2854	*v* (C-H) alkyl chains, str
1572, 1468	1574, 1470	Imidazole ring skeleton, str sym
1350	1352	$v(SO_2)$, str asym
1192	1198	$v(CF_3)$, str asym
1136	1138	$v(SO_2)$, str sym
1057	1059	*v*(SNS), str asym

[a] Abbreviations: str, stretching; sym, symmetrical; asym, asymmetrical.

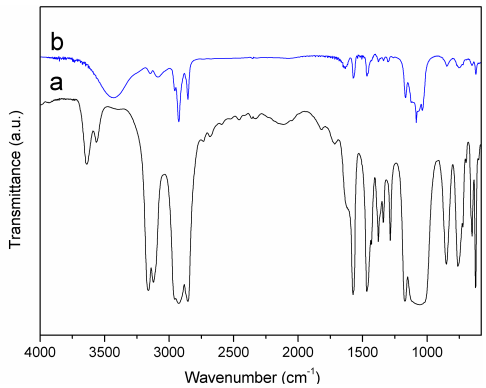

Fig. S9 FT-IR spectra of (a) the pure $[C_{10}mim][BF_4]$ and (b) the Ag cubes/$[C_{10}mim][BF_4]$.

Table S4. The main FTIR absorption bands of pure $[C_{10}mim][BF_4]$ and Ag cubes/$[C_{10}mim][BF_4]$[a]

Wavelength of the bands (cm^{-1})		
Pure $[C_{10}mim][BF_4]$	Ag cubes/$[C_{10}mim][BF_4]$	Vibration
3161, 3122	3145, 3086	*v* (C-H) imidazole ring, str
2956, 2926, 2854	2956, 2926, 2854	*v* (C-H) alkyl chains, str
1574, 1468	1574, 1466	Imidazole ring skeleton, str sym
1059	1062	*v*(B-F), str

[a] Abbreviations: str, stretching; sym, symmetrical.

References

[1] (a) P. Bonhote, A. Dias, N. Papageorgiou, K. Kalyanasundaram and M. Gratzel, *Inorg. Chem.*, 1996, **35**, 1168; (b) J. G. Huddleston, A. E. Visser, W. M. Reichert, H. D. Willauer, G. A. Broker and R. D. Rogers, *Green Chem.*, 2001, **3**, 156; (c) B. D. Fitchett, J. B. Rollins and J. C. Conboy, *Langmiur*, 2005, **21**, 12179; d) J. D. Holbrey and K. R. Seddon, *Dalton Trans.*, 1999, **27**, 2133.

[2] (a) A. Dawn, P. Mukherjee and A. K. Nandi, *Langmuir*, 2007, **23**, 5231; (b) Y. Tan, F. Bai, D. Wang, Q. Peng, X. Wang and Y. Li, *Chem. Mater.*, 2007, **19**, 5773; (c) M. Mazur, *J. Phys. Chem. C*, 2008, **112**, 13528.

[3] (*a*) R. C. Jin, Y. C. Cao, C. A. Mirkin, K. L. Kelly, G. C. Schatz and J. G. Zheng, *Science*, 2001, **294**, 1901; (*b*) R. C. Jin, Y. C. Cao, E. C. Hao, G. S. Métraux, G. C. Schatz and C. A. Mirkin, *Nature*, 2003, **425**, 487; (*c*) Y. Sun, B. Mayers and Y. Xia. *Nano Lett.*, 2003, **3**, 675; (*d*) I. Washio, Y. Xiong, Y. Yin and Y. Xia, *Adv. Mater.*, 2006, **18**, 1745; (*e*) X. Bai, L. Zheng, N. Li, B. Dong and H. Liu, *Cryst. Growth Des.*, 2008, **8**, 3840.

[4] (*a*) P. Jiang, J. J. Zhou, R. Li, Y. Gao, T. L. Sun, X. W. Zhao, Y. J. Xiang and S. S. Xie, *J. Nanopart. Res.*, 2006, **8**, 927; (*b*) D. Aherne, D. M. Ledwith, M. Gara and J. M. Kelly, *Adv. Funct. Mater.*, 2008, **18**, 2005; (*c*) Y. Sun and C. An, *Front. Mater. Sci.*, 2011, **5**, 1.

[5] J. Yang, L. Lu, H. Wang, W. Shi and H. Zhang, *Cryst. Growth Des.*, 2006, **6**, 2155.

[6] (a) Y. Sun and Y. Xia, *Science*, 2002, **298**, 2176; (b) S, H, Im, Y. T. Lee, B. Wiley and Y. Xia, *Angew. Chem. Int. Ed.*, 2005, **44**, 2154; (c) A. R. Siekkinen, J. M. McLellan, J. Chen and Y. Xia, *Chem. Phys. Lett.*, 2006, **432**, 491.

[7] (a) Q. Zeng, X. Jiang, A. Yu and G. Lu, *Nanotechnology*, 2007, **18**, 035708; (b) X. Bai, Y. Gao, H. Liu and L. Zheng, *J. Phys. Chem. C*, 2009, **113**, 17730.

[8] (a) Y. Zhou, J. H. Schattka and M. Antonietti, Nano Lett., 2004, 4, 477; (b) J. Lian, T. Kim, X. Liu, J. Ma and W. Zheng, *J. Phys. Chem. C*, 2009, **113**, 9135.